Proceedings World Geothermal Congress 2000
Kyushu - Tohoku, Japan, May 28 - June 10, 2000

ELETROMAGNETIC TOMOGRAPHY USING SURFACE SOURCES AND BOREHOLE RECEIVERS IN KAKKONDA

Kazumi Osato[1] and Takao Ominato[2]
[1]Geothermal Energy Research and Development Co., ltd., 11-7 Kabuto-cho, Nihonbashi, Chuo-ku, Tokyo, Japan
[2]New Energy and Industrial Technology Development Organization, 3-1-1 Higashiikebukuro, Toshima-ku, Tokyo, Japan
(Now: Earthquake Research Institute, University of Tokyo, 1-1-1, Yayoi, Bunkyo-ku, Tokyo, Japan)

Key Words: geothermal, geophysics, electromagnetic, resistivity, tomography, Kakkonda

ABSTRACT

NEDO has been undertaking the Deep Seated Geothermal Resources Survey Project in Kakkonda (Iwate, Japan) since 1992. The pilot survey well WD-1a reached 3,729 m and over 500 degrees C in FY1995. In FY1996, NEDO drilled a sidetracking well WD-1b and hit several high permeability zones. We developed a new exploration technique using borehole to surface electro-magnetic tomography system named VEMP (Vertical ElectroMagnetic Profiling) under this project (Miura et al., 1995). We applied it to a test survey at the open-hole section (2,250 to 2,850 meters) of WD-1b in 1997. We measured magnetic fields (horizontal fields toward transmitters and vertical fields) at six frequencies (1,4,16,32,64 and 128Hz) at 13 depth levels in the hole. Signal sources were grounded-wires at six locations on the ground surface. For interpretation of the data, we are developing 2.5-D FEM non-linear least square inversion code including robust weighting for the field data. The initial model for the inversion was based on the 2-D inversion result that was obtained by MT/CSAMT sounding in 1994 (Yamane et al., 1996).

1. INTRODUCTION

Surveys of deep-seated geothermal resources become increasingly more difficult than conventional (shallow) geothermal resources, as the exploration depth increases. The MT method has been employed extensively to infer geothermal structures by investigating the resistivity structure at great depths. MT, being a ground surface surveying method, is able to provide information of electric resistivity distribution at a large depth. However, the area where MT can be applied is relatively limited. It is considered to be possible to utilize the advantages of both a ground surface method and borehole survey methods by putting the following three methods in practice.

1) Single hole electromagnetic method to explore the vicinity of the borehole.
2) Surface to borehole electromagnetic method to explore the area surrounded by surface sources and borehole receivers.
3) Surface electromagnetic sounding method (MT) to explore the deep and wide area.

The first experimental data obtained from the deep exploration hole that will be drilled in a geothermal field can be used as a control data for these methods. It will improve the accuracy of the resistivity structure.

2. FIELD EQUIPMENT

Figure 1 shows the schematic diagram of the VEMP system (ELECTROMAGNETIC INSTRUMENT Inc.). The system was based on frequency domain controlled source EM method. The receiver system consists of tri-axial borehole induction magnetometer, a metal dewar flask with an orientation sensor (magnetic and accelerometer) and electronic devices (amplifiers, synchronous detector, ADC, and data-encoder), a winch unit of seven-conductor armored cable, a surface interface unit with PC, and a rubidium clock for synchronization with the transmitter system. The transmitter system consists of a CSAMT transmitter (30kVA), a transmitter controller, a surface interface unit with PC, and a rubidium clock. The CSAMT transmitter can supply a current either a loop source or a grounded wire with maximum current of 20A and at multi-frequencies (1, 2, 4, 8, 16, 32, 64, and 128 Hz). The borehole tool can be used in high-temperature geothermal wells (maximum temperature = 260 degrees C and maximum pressure = 40 MPa). (Miura el al., 1996)

3. NUMERICAL SCHEME

The numerical method to interpret the recorded data is as follows;

(1) The numerical method for forward calculation is based on 2.5 dimensional (2D structure and 3D source) finite element method for EM fields (Lee and Morrison, 1985)
(2) The inversion scheme is based on non-linear least squares method with regularizing optimization by robust estimation.

Numerical solutions for the 2-1/2-D EM problem have been presented by Stoyer and Greenfield (1976), Lee and Morrison (1885), and recently by Unsworth et al. (1993). In all these solutions the dependence in the strike direction, say y, has been transformed out, so that the resulting Maxwell's equations are independent from the strike.

In this way the original problem is reduced to 2-D for each Fourier wavenumber (k_y). One can then algebraically manipulate and reformulate the problem using only two fields (E_y and H_y) that are parallel to strike.

Upon solving for these two components numerically, the other components can be obtained by taking appropriate spatial derivatives of these two. The spatial derivatives often introduce numerical errors, and for this reason, Lee and Morrison (1985) formulated the problem using full vector (3-component) electric field. Even with this approach it has been pointed out that there are considerable numerical errors in the numerically computed magnetic fields. One obvious reason for this numerical error, in addition to the numerical derivatives, seems to have resulted from the fact that electric field normal to a boundary between different conductivity is discontinuous. For this and other reasons described in this numerical scheme we choose to develop the solution using three-components of magnetic field (H_x, H_y, and H_z).

3.1 Formulation of the 3-D problem and reduction to 2-D

Maxwell's equations in the frequency domain ($e^{i\omega t}$) with external sources are

$$\nabla \times \mathbf{E} = -i\omega\mu(\mathbf{H} + \mathbf{M}). \quad (1)$$

$$\nabla \times \mathbf{H} = (\sigma + i\omega\varepsilon)\mathbf{E} + \mathbf{J}. \quad (2)$$

Here, M and J are the magnetic and electric sources,

respectively. In practice, only one source will be used in the next formulation process. By eliminating E from (1) and (2), we obtain

$$\nabla \times \left(\frac{1}{(\sigma + i\omega\varepsilon)} \nabla \times H \right) = -i\omega\mu H + S, \quad (3)$$

where the source term on the right is given by

$$S = \nabla \times \left(\frac{J}{\sigma + i\omega\varepsilon} \right),$$

in case for the electric source only, and

$$S = -i\omega\mu M ,$$

in case for the magnetic source only.

Using Fourier transformation $(y \rightarrow k_y)$

$$\tilde{H}(x, k_y, z) = \int_0^{\infty} H(x, c, z) e^{-ik_y y} dy,$$

and the fact that electrical conductivity is constant in y, and $\frac{\partial}{\partial y}(\cdot) = ik_y(\cdot)$ in the transformed domain, we find

Fourier transform $\{ y \rightarrow k_y \}$ of $\left\{ \nabla \times \left(\frac{1}{(\sigma + i\omega\varepsilon)} \nabla \times H \right) \right\}$

$$= \left(\frac{ik_y}{(\sigma + i\omega\varepsilon)} \left(\frac{\partial \tilde{H}_y}{\partial x} - ik_y \tilde{H}_x \right) - \frac{\partial}{\partial z} \left(\frac{1}{(\sigma + i\omega\varepsilon)} \left(\frac{\partial \tilde{H}_x}{\partial z} - \frac{\partial \tilde{H}_z}{\partial x} \right) \right) \right) \tilde{i}$$

$$+ \left(\frac{\partial}{\partial z} \left(\frac{1}{(\sigma + i\omega\varepsilon)} \left(ik_y \tilde{H}_z - \frac{\partial \tilde{H}_y}{\partial z} \right) \right) - \frac{\partial}{\partial x} \left(\frac{1}{(\sigma + i\omega\varepsilon)} \left(\frac{\partial \tilde{H}_y}{\partial x} - ik_y \tilde{H}_x \right) \right) \right) \tilde{j}$$

$$+ \left(\frac{\partial}{\partial x} \left(\frac{1}{(\sigma + i\omega\varepsilon)} \left(\frac{\partial \tilde{H}_x}{\partial z} - \frac{\partial \tilde{H}_z}{\partial x} \right) \right) - \frac{ik_y}{(\sigma + i\omega\varepsilon)} \left(ik_y \tilde{H}_z - \frac{\partial \tilde{H}_y}{\partial z} \right) \right) \tilde{k}.$$

From equation (3), by matching terms, we get

$$\frac{ik_y}{(\sigma + i\omega\varepsilon)} \left(\frac{\partial \tilde{H}_y}{\partial x} - ik_y \tilde{H}_x \right) - \frac{\partial}{\partial z} \left(\frac{1}{(\sigma + i\omega\varepsilon)} \left(\frac{\partial \tilde{H}_x}{\partial z} - \frac{\partial \tilde{H}_z}{\partial x} \right) \right) + i\omega\mu \tilde{H}_x = \tilde{S}_x \quad (4)$$

$$\frac{\partial}{\partial z} \left(\frac{1}{(\sigma + i\omega\varepsilon)} \left(ik_y \tilde{H}_z - \frac{\partial \tilde{H}_y}{\partial z} \right) \right) - \frac{\partial}{\partial x} \left(\frac{1}{(\sigma + i\omega\varepsilon)} \left(\frac{\partial \tilde{H}_y}{\partial x} - ik_y \tilde{H}_x \right) \right) + i\omega\mu \tilde{H}_y = \tilde{S}_y \quad (5)$$

$$\frac{\partial}{\partial x} \left(\frac{1}{(\sigma + i\omega\varepsilon)} \left(\frac{\partial \tilde{H}_x}{\partial z} - \frac{\partial \tilde{H}_z}{\partial x} \right) \right) - \frac{ik_y}{(\sigma + i\omega\varepsilon)} \left(ik_y \tilde{H}_z - \frac{\partial \tilde{H}_y}{\partial z} \right) + i\omega\mu \tilde{H}_z = \tilde{S}_z \quad (6)$$

Applying Galerkin's method, and using integral by parts, we obtain

$$\int_S \left(\frac{ik_y}{(\sigma + i\omega\varepsilon)} \left(\frac{\partial \tilde{H}_y}{\partial x} - ik_y \tilde{H}_x \right) \varphi_i + \frac{1}{(\sigma + i\omega\varepsilon)} \left(\frac{\partial \tilde{H}_x}{\partial z} - \frac{\partial \tilde{H}_z}{\partial x} \right) \frac{\partial \varphi_i}{\partial z} + i\omega\mu \tilde{H}_x \varphi_i \right) ds$$

$$= \int_S \tilde{S}_x \varphi_i ds \quad (7)$$

$$\int_S \left(\frac{1}{(\sigma + i\omega\varepsilon)} \left(\frac{\partial \tilde{H}_y}{\partial x} - ik_y \tilde{H}_x \right) \frac{\partial \varphi_i}{\partial x} - \frac{1}{(\sigma + i\omega\varepsilon)} \left(ik_y \tilde{H}_z - \frac{\partial \tilde{H}_y}{\partial z} \right) \frac{\partial \varphi_i}{\partial z} + i\omega\mu \tilde{H}_y \varphi_i \right) ds$$

$$= \int_S \tilde{S}_y \varphi_i ds \quad (8)$$

$$\int_S \left(\frac{1}{(\sigma + i\omega\varepsilon)} \left(\frac{\partial \tilde{H}_x}{\partial z} - \frac{\partial \tilde{H}_z}{\partial x} \right) \frac{\partial \varphi_i}{\partial x} + \frac{ik_y}{(\sigma + i\omega\varepsilon)} \left(ik_y \tilde{H}_z - \frac{\partial \tilde{H}_y}{\partial z} \right) \varphi_i - i\omega\mu \tilde{H}_z \varphi_i \right) ds$$

$$= -\int_S \tilde{S}_z \varphi_i ds \quad (9)$$

The tensor test function used in these equations are identical to the one used for the 3-D problem. Only difference here is that these functions are 2-D defined in the *x-z* plane.

3.2 Finite element equation

The numerical domain is first divided into N rectangular elements. The magnetic field is assumed to be bi-linear, and we use the same test function as the base function to describe the field inside each of the rectangle.

$$H_i^h(x, y, z) = \sum_{j=1}^{4} H_i \varphi_j(x, y, z), \quad i = x, y, \text{or} z \quad (10)$$

Here the base function is assumed to be bi-linear as

$$\varphi_i = a_i + b_i x + c_i z + d_i xz, \quad i = 1, 2, 3, \text{and} 4 . \quad (11)$$

Detailed process for deriving coefficients of the base function is referred to Zienkiewicz (1971). If we consider a rectangle with four corners numbered 1, 2, 3, and 4,

The coefficients for the base function are given as

$$\begin{bmatrix} a_1 & a_2 & a_3 & a_4 \\ b_1 & b_2 & b_3 & b_4 \\ c_1 & c_2 & c_3 & c_4 \\ d_1 & d_2 & d_3 & d_4 \end{bmatrix} = \begin{bmatrix} 1 & x_1 & y_1 & x_1 y_1 \\ 1 & x_2 & y_2 & x_2 y_2 \\ 1 & x_3 & y_3 & x_3 y_3 \\ 1 & x_4 & y_4 & x_4 y4 \end{bmatrix}^{-1} \quad (12)$$

3.3 Integral boundary condition

In the wavenumber domain (k_y), the integral boundary condition on the earth surface looks like

$$\tilde{H}(x, k_y, z) = M \tilde{H}(x, k_y, z) + \int_1 \frac{1}{i\omega\varepsilon} (\nabla \times \tilde{G} \times \tilde{H})_z dx$$

$$- \int_1 \frac{1}{(\sigma + i\omega\varepsilon)} \left(\left(ik_y \tilde{H}_z - \frac{\partial \tilde{H}_y}{\partial z} \right) \tilde{G}_y - \left(\frac{\partial \tilde{H}_x}{\partial z} - \frac{\partial \tilde{H}_z}{\partial x} \right) \tilde{G}_x \right) dx, \quad (13)$$

3.4 Inverse Fourier transform

Equations (7), (8), and (9), after modified by the integral boundary condition (13), will result a system of linear equations in the wavenumber domain.

$$K \cdot \tilde{H} = S \quad . \quad (14)$$

The source term on the right of this equation consists of contributions from integral boundary condition, boundary values prescribed on the boundaries in the lower half space. Numerical solution obtained from this equation is in the wavenumber (k_y) domain and they need to be inversely Fourier -transformed.

$$H(x, y, z) = \frac{1}{2\pi} \int_0^{\infty} \tilde{H}(x, k_y, z) e^{ik_y y} dk_y \quad (15)$$

3.5 Inversion scheme

The core portion of the inversion code uses the Householder algorithm (Press et al., 1988). This algorithm requires the Jacobian (sensitivity) matrix and it hence requires a great deal of memory and computation time if we use the normal Householder algorithm. Therefore, our code uses the incomplete Cholesky conjugate gradient (ICCG) algorithm (Press et al., 1988; Mackie and Madden, 1993) to reduce the required memory and computation time.

The inversion involves the following regularizing optimization process.

$$\left\| W_d (H_d - H_m) \right\|^2 + \alpha (R(\sigma), \sigma) = \min . \quad (16)$$

where subscripts '*d*' and '*m*' indicate data and a model results, respectively, the symbol 'α' the regularizing parameter, and the weighting matrix W_d. The weighting matrix is defined as a diagonal matrix

$$W_d = D\{(1 - \chi_1^{NR})(1 - \chi_1^{NI}), \ldots, (1 - \chi_i^{NR})(1 - \chi_i^{NI}), \ldots, (1 - \chi_M^{NR})(1 - \chi_M^{NI})\} \quad (17)$$

Here we assume there are a total of M data. The symbols used are normalized standard deviations defined as

$$\chi_i^{NR} = \frac{\chi_i^R}{\max\{\chi_j^R, \chi_j^I; j = 1, M\}},$$

$$\chi_i^{NI} = \frac{\chi_i^I}{\max\left\{\chi_j^R, \chi_j^I;\ j = 1, M\right\}}, \quad (18)$$

The standard deviations used in (18) are obtained from

$$\chi_i^R = \sqrt{\frac{1}{2}\left\{\left(\frac{H_i^e}{H_i} - m(\chi_i^R)\right)^2 + \left(\frac{\phi_i^e}{\phi_i} - m(\chi_i^R)\right)^2 + \left(\frac{RH_i^e}{RH_i} - m(\chi_i^R)\right)^2\right\}},$$

$$\chi_i^I = \sqrt{\frac{1}{2}\left\{\left(\frac{H_i^e}{H_i} - m(\chi_i^I)\right)^2 + \left(\frac{\phi_i^e}{\phi_i} - m(\chi_i^I)\right)^2 + \left(\frac{IH_i^e}{IH_i} - m(\chi_i^I)\right)^2\right\}}. \quad (19)$$

Symbols used in this equation are

$$m(\chi_i^R) = \frac{1}{3}\left(\frac{|H_i^e|}{|H_i|} + \frac{|\phi_i^e|}{|\phi|} + \frac{|RH_i^e|}{|RH_i|}\right),$$

$$m(\chi_i^I) = \frac{1}{3}\left(\frac{|H_i^e|}{|H_i|} + \frac{|\phi_i^e|}{|\phi_i|} + \frac{|IH_i^e|}{|IH_i|}\right). \quad (20)$$

In equations (19) and (20), H_i and H_i^e are magnetic field at the i-th position and its estimated error, ϕ_i and ϕ_i^e are magnetic field phase and error, RH_i and RH_i^e are the real component of the magnetic field and its error, and finally, IH_i and IH_i^e are the imaginary component of the magnetic field and its error, respectively.

4. CASE STUDY IN THE KAKKONDA GEOTHERMAL FIELD

NEDO has been undertaking the Deep Seated Geothermal Resources Survey Project in Kakkonda (Iwate, Japan) since 1992. The pilot survey well WD-1a reached 3,729 m and encountered a very high temperature of over 500 degrees C in FY1995 (Uchida, et al., 1996). In FY1996, NEDO drilled a sidetracking well WD-1b and it encountered several high permeability zones. Many geophysical surveys (MT/CSAMT (Yamane et al., 1996, Ogawa et al., 1997), reflection seismic (NEDO, 1995), micro-earthquake, etc.) and geophysical logging were carried out in this field. The VEMP survey was applied at the open-hole section (2,250 to 2,850 meters) of WD-1b in 1997. Figure 2 shows the location map of the grounded-wire sources (G1, G2, G3, G4, G5, and G9) and the well head of WD-1b. The measurement of three component magnetic fields at six sources was done every 50 meters depth between 2,250 meters to 2,850 meters of WD-1b. Frequencies of the signals were 1, 2, 4, 8, 16, 32, 64, and 128 Hz.

The Kakkonda geothermal field, which is one of the active geothermal fields in the Sengan volcanic region, is located in the Kakkonda valley. The subsurface geology of the field is composed of the Yamatsuda Formation, Takinoue-onsen F., Kunimitoge F., Obonai F., and Pre-Tertiary formation in descending order. The geothermal reservoir in Kakkonda consists of the shallow reservoir and deep reservoir. These two reservoirs are separated at ca.1.5 km and characterized by a large difference in permeability and temperature(Doi et al., 1995; Kato et al., 1996). The permeability is different by two-orders of magnitude between the shallow and deep reservoir (Kajiwara et al., 1993). Recently, a highly permeable zone in the deep reservoir was found at the margin of the neo-granite pluton (the Kakkonda Granite) which was embedded below 1.95 km depth. Muraoka et al. (1995) referred to the reservoir at the margin of a pluton as a plutonic-rim reservoir.

In the numerical model, x direction was defined as the direction of G1-G5 line (Southeast: positive). The receiver hole (WD-1b) was coordinated at (-500, 0, 0) [meters]. Since the shallower section, upper 2,250 meters, was cased by steel casing and no data was recorded in the survey, the initial model for the inversion was based on the 2-D resisitivity section of the MT/CSAMT data were obtained in 1994 as a part of this project. Figure 3 (1) shows the 2-D inverted resisitivity section that was interpreted by the Generalized Rapid Relaxation Inversion method (Yamane et al., 1996). The resistivity values of the initial model were re-sampled to match to 2-D FEM nodes that defined for this analysis. The resistivity image was obtained by 2.5-D FEM non-linear inversion that used six grounded-wire sources at six frequencies (1Hz, 4Hz, 16Hz, 32Hz, 64Hz and 128Hz) and magnetic field data (Hx and Hz) at 13 receivers (2,250 meters to 2,850 meters). Since some data was of bad quality, we did not use 50% of them as shown in Table 1. Figure 3 (2), (3) shows some images of 2.5D inversion during eight times of iteration. Figure 3 (4) shows the RMS error in the progress of iteration. The RMS error decreased from the 1st inversion to the 7th inversion and increased at the 8th inversion. The computation time was 86.3 hours on an Alpha-chip processor (DIGITAL Alpha 21264/500MHz chip with 1024MB).

Figure 4 shows the comparison of the inverted resistivity image of the VEMP data with the geological cross-section (Doi et al., 1995) (4), the electrical logging data (1), the inverted 2D image of the MT/CSAMT data in 1994 (2) and the reflection seismic cross-section (3). The resistivity distribution was obtained by 3D interpolation of 44 electrical logging (Long Normal) data (NEDO and JMC). The reflection seismic cross-section was surveyed in 1994 as a part of the NEDO project – "Development of exploration methods for fracture-type geothermal reservoir" (NEDO, 1995).

The characteristics of the inverted resistivity image of the VEMP data are as follows;

(1) The shape of the Kakkonda Granite that was confirmed by drilling was interpreted as a high resistivity zone. It was similar to the interpolated distribution of the electrical logging data (44 wells). That was also similar to the deep horizon identified by the reflection seismic survey.
(2) The shallower part of electrical logging data has very conductive, however, a high resisivity region was found at the deeper part of western side of WD-1a/WD-1b (left hand of Figure 4(4)).
(3) At the shallow part of southeastern side (right hand of Figure 4(4)), a high resistivity region was identified. This area was interpreted as the location of Torigoeno-taki Dacite Intrusion.
(4) The shape of conductive zone in shallow part is

harmonized with the shape of the weak reflective region of the seismic survey. This zone seems to match to the iso-contour below 200 degrees C obtained by intrusions and minimum homogenization temperature of fluid inclusions.

(5) The electrical logging data near WD-1a/WD-1b shows lower resistivity than the VEMP survey from 200 to 1,000 meters TD. The result of MT surveys in this field (Yamane et al., 1996; Ogawa et al., 1997) shows also higher than the electrical logging from 200 to 1,600 meters TD. By their recent 2-D and 3-D analyses of the MT surveys, the high resistivity zone at same depth was found out in southern side of the Kakkonda river. Since the VEMP 2.5-D analysis is based on 2-D structure, the higher resistivity from 200 to 1,000 meters can be assumed as the effect from this 3-D structure.

5. DISCUSSION AND CONCLUSION

All resistivity surveys (VEMP, MT, and logging) show conductive (below 20-30 ohm-m) in range of below 200 degrees C in the Kakkonda reservoir. Montmorillonite is one of the most interest 'key' minerals that show very conductive. This seals the cap-rock formation and it is created in the condition of below 150 degrees C. Uchida et al. (1990) described that the bottom of lower resistivity zone obtained from the EMAP and the Schlumberger in Mt. Akita-Yakeyama of Sengan volcanic area indicated iso-contour of 200 degrees C and it formed the cap-rock. The very shallow resistivity structure of the Kakkonda reservoir is similar to this phenomenon and indicates the sealing zone (cap-rock). In the deep resistivity structure of the VEMP survey, we found more conductive zone (200 – 300 ohm-m) at the rim of the Kakkonda granite than very highly resistivity zone in the granite (>400 ohm-m). This zone is dived and lapses into the highly resistivity zone at western side of WD-1a/WD-1b and bounded the reservoir. All deep fracture zones that were identified by loss-water zone during drilling are located in this zone. By the electrical logging, we could also prove this structure but the surface electromagnetic sounding survey (MT/CSAMT) was more difficult to identify it clearly.

ACKNOWLEDGMENTS

This works is funded by MITI's New Sunshine Project. The authors wish to express their deep gratitude to Japan Metal and Chemical Co. and Geothermal Engineering Co. (Japan) for their advice with the field data, Dr. Yoonho Song (Korea Institute of Geology, Korea) for his theoretical support, and ELECTROMAGNETIC INSTURUMENT Inc. (USA) for their technical support.

REFERENCES

Doi, N., Muramatsu, Y. Chiba, Y. and Tateno, M., 1988, Geological analysis of the Kakkonda geothermal reservoir, Proc. Int.Sym. on Geothermal Energy,1988, Kumamoto and Beppu, Japan, 522-525.

Doi, N, Kato, O., Kanisawa, S. and Ishikawa, K. 1996, NEO-TECTONICS FRACTURING AFTER EMPLACEMENT OF QUATERNARY GRANITIC PLUTON IN THE KAKKONDA GEOTHERMAL FIELD, GRC TRANS-ACTIONS, vol.19 .

Kajiwara, T., Hanano, M., Ikeuchi, K. and Sakagawa, Y., 1993, Permeability structure at the Kakkonda geothermal field, Iwate Prefecture, Japan: Abst. 1993 Ann. Meeting, Geother. Res, Soc, Japan, B30 (in Japanese)

Kanisawa, S. Doi, N., Kato, O., ans Ishikawa, K. (1994): Quaternary Kakkonda Grinite underlyning the Kakkonda geothermal field, northeast Japan: J. Mineral. Petrol. Encon. Geol., vol.89, pp.390-407 (in Japanese)

Kato, O., Doi, N., Ikeuchi, K. , Kondo, T., Kamenosono, H., Yagi, M. and Uchida, T. (1996): Characteristics of temperature curves and fracture systems in Quaternary granite and Tertiary pyroclastic rocks of NEDO WD-1a in Kakkonda geothermal field, Japan, Proc. 8th Int. Sym. on the OCCTD, pp.241-246.

Jacobs, D. A. H., 1986, A Generalization of the Conjugate-Gradient Method to Solve Complex Systems, IMA Journal of Numerical Analysis, vol.6, pp.447-452.

Lee, K. H. and Morrison, H. F., 1985, A numerical solution for the electromagnetic scattering by a two-dimensional inhomogeneity: Geophysics, vol.50, pp.466-472.

Mackie, R. L., and Madden, T. R., 1993, Three-dimensional magnetotelluric inversion using conjugate gradients, Geophys. J. Int., 115,pp. 215-229.

Miura, Y., Osato, K., Takasugi, S. Muraoka, H. and Yasukawa, K. ,1996, Development of the Vertical ElectroMagnetic Profiling (VEMP) method, J.A.G., vol.35, pp.191-197.

Muraoka, H., Yagi, M., Yasukawa, K. Hishatani, K. Doi, N., and Miyazaki, S., 1995, NEDO 'Deep-seated geothermal resources survey': a link of igneous, metamorphic and hydrothermal processes: Proc. World Geother. Con., 1995, Florence, pp.1509-1514.

NEDO, 1995, Annual report in FY1994 for "Confirmation Study of the Effectiveness of Prospecting Techniques for Deep Geothermal Resources – Development of exploration methods for fracture-type geothermal reservoir " , 239pp.. (in Japanese)

Ogawa, Y., Uchida, T., and Takakura, S., 1997, MT survey-ing in the Kakkonda geothermal area, Proc. of the 96th SEGJ Conference, pp.265-270. (in Japanease)

Press, W. H., Flannery, B. P., Teukolsky, S. A., and Vetterling, W. T., 1988, Numerical Recipes: The Art of Scientific

Computing, Cambridge University Press.

Stoyer, C. H. and Greenfield R .J., 1976, Numerical solutions of the response of a two-dimensional earth to an oscillating magnetic dipole source: Geophysics, 41, pp.519-530.

Unsworth, M.J., Travis, B.J., and Chave, A.D., 1993, Electromagnetic induction by a finite electric dipole source over a 2-D earth: Geophysics, 58, p.198-214.

Uchida, T, 1990, Reservoir Structure of the Sengan Geothermal Field Interpreted from the Resisitivity Data, J. of Geother. Rese. Soc. of Japan, vo.12, No.2, 41, pp.1-21. (in Japanese)

Uchida, T., Akaku, K., Sasaki, M., Kamenosono, H., Doi, N., and Miyazaki, S., 1996, Recent Progress of NEDO's "Deep-Seated Geothermal Resources Survey" Project, GRC TRANSACTIONS, Vo.20

Yamane, K., Takasugi, S. Miyazaki. S., and Uchida, T., 1996, MT2-D inversion analysis in Kakkonda geothermal field, Proc. of the 94th SEGJ Conference, pp.276-280. (in Japanese)

Zienkiewicz, O. C., 1971, The Finite Element Method in Engineering Science: London, McGraw-Hill.

Table 1. Applied frequency (O) for inversion

Source Freq.	G 1	G2	G3	G4	G9	G5
1 Hz	O	O	O	O	O	O
2 Hz	X	O	O	O	O	O
4 Hz	X	X	X	X	X	X
8 Hz	X	X	X	X	X	X
16 Hz	O	O	O	O	X	X
32 Hz	X	X	O	O	O	O
64 Hz	X	X	X	O	O	O
128Hz	X	X	X	X	O	O

O: used, X: not-used

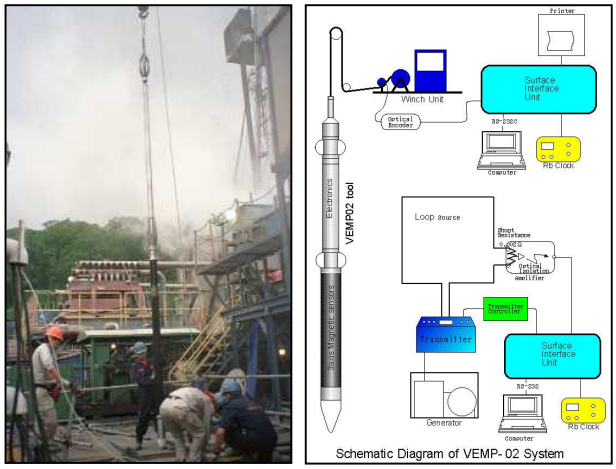

Figure 1. Schematic diagram and picture of the VEMP system

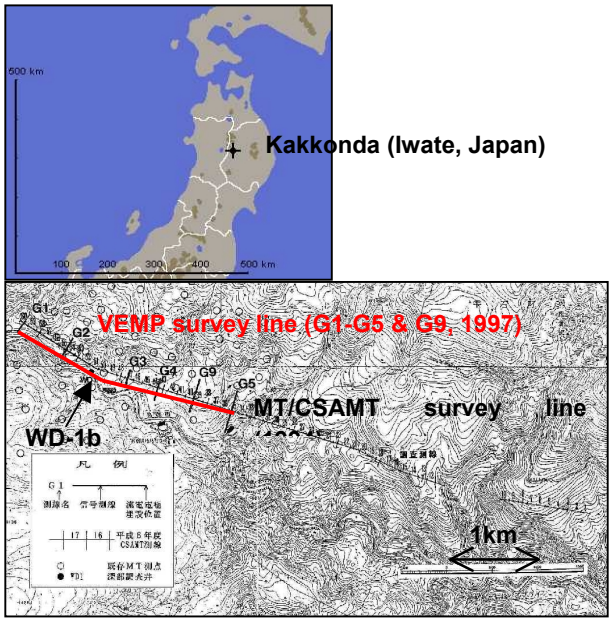

Figure 2. Layout of surface sources for the VEMP survey (G1, G2, G3, G4, G5, and G9 are the grounded wire lines), the MT/CSAMT survey line in 1994, and WD-1b.

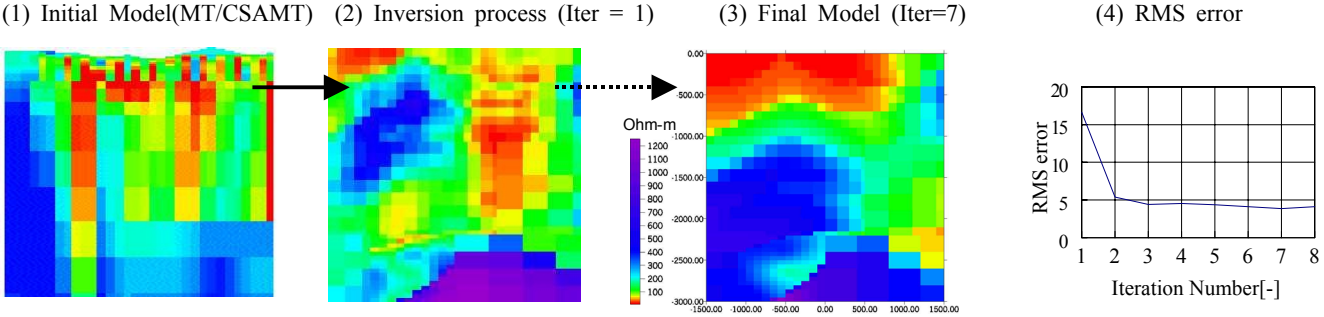

Figure 3. 2D resistivity image obtained from MT/CSAMT survey in 1994 (Yamane et al., 1996) for the initial model and the 2.5-D resistivity images (unit: ohm-m) of the VEMP survey in Kakkonda obtained at each iteration process (Iteration = 1 and 7)

(1) The interpolated resistivity cross section obtained by the electrical logging data (long normal)

(2) The inverted resistivity image obtained by 2-D inversion of MT/CSAMT (Yamane et al., 1996)

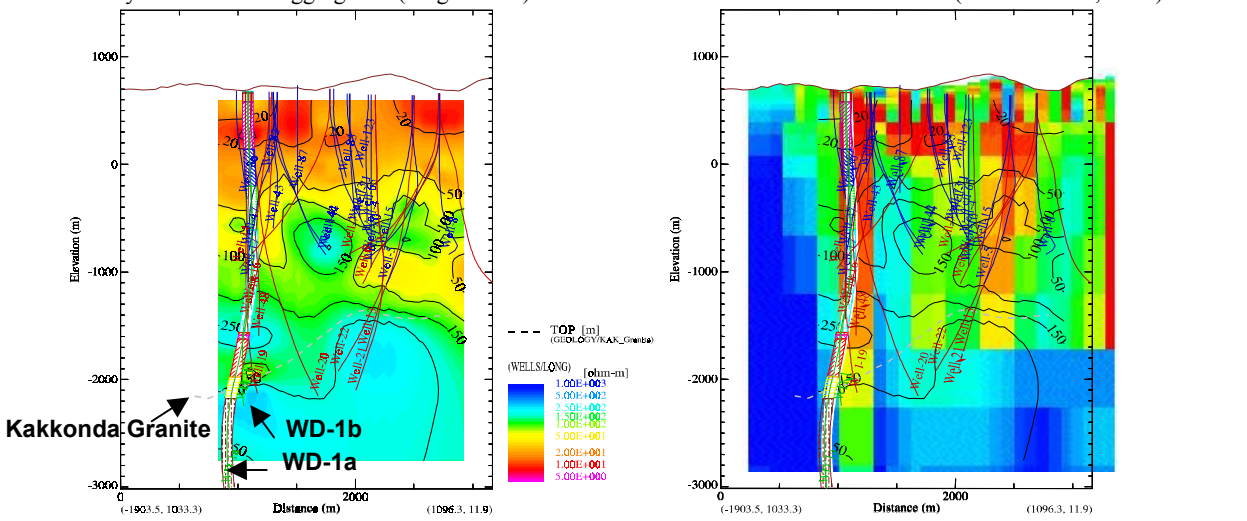

(3) Geologic interpretation of seismic section (NEDO, 1995) with well trajectories

(4) The inverted resistivity image of the VEMP 2.5D inversion and the geological section in Kakkonda (modified Doi et al, 1995)

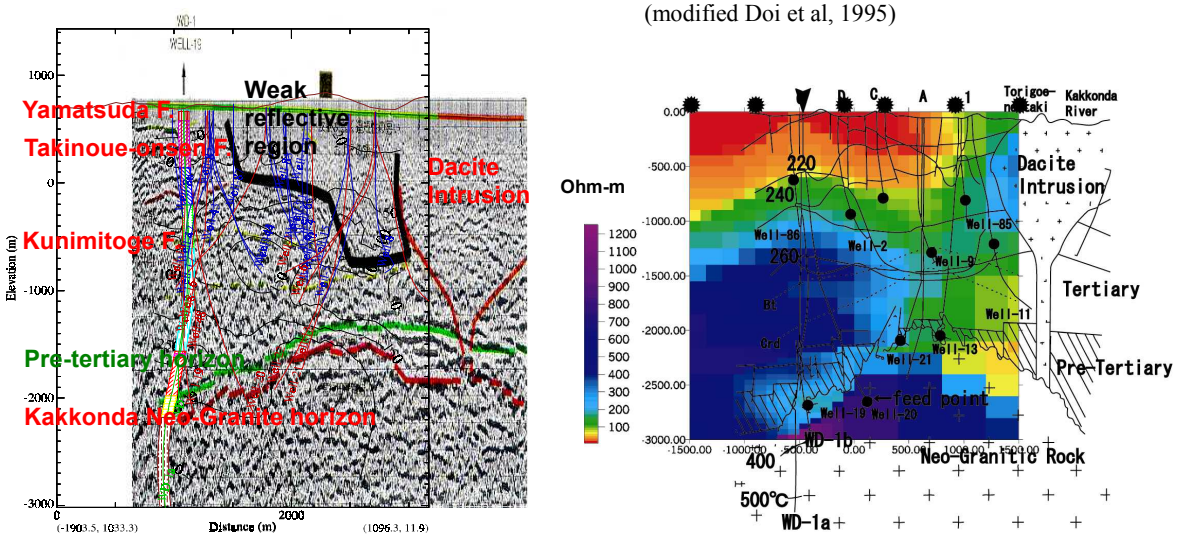

Figure 4. Comparison of the interpolated resistivity distribution obtained by the electrical logging data (JMC and NEDO), the MT 2-D inverted resistivity image (Yamane et al., 1996), the seismic cross section (NEDO, 1995) and the 2.5-D inverted resistivity image obtained by the VEMP data in Kakkonda (NW-SE cross section)